International Journal of Bifurcation and Chaos, Vol. 21, No. 7 (2011) 1895–1905

DOI: 10.1142/S0218127411029483

# ASYMMETRIC TRANSITION AND TIME-SCALE SEPARATION IN INTERLINKED POSITIVE FEEDBACK LOOPS

PENCHO YORDANOV
*School of Engineering and Science,*
*Jacobs University Bremen, Campus Ring 1,*
*28759 Bremen, Germany*
*p.yordanov@jacobs-university.de*

STEFKA TYANOVA
*Computational Genomics Group, TU München,*
*Am Forum 1, 85354 Freising, Germany*
*tyanova@wzw.tum.de*

MARC-THORSTEN HÜTT
*School of Engineering and Science,*
*Jacobs University Bremen, Campus Ring 1,*
*28759 Bremen, Germany*
*m.huett@jacobs-university.de*

ANNICK LESNE
*Institut des Hautes Études Scientifiques,*
*35 route de Chartres, F-91440 Bures-sur-Yvette, France*
*LPTMC UMR 7600, Université Pierre et Marie Curie,*
*4 Place Jussieu, F-75252 Paris, France*
*lesne@lptmc.jussieu.fr*

Received June 4, 2010; Revised January 12, 2011

In [Brandman *et al.*, 2005] it was proposed that interlinked fast and slow positive feedback loops are a frequent motif in biological signaling, because such a device can allow for a rapid response to an external stimulus (sensitivity) along with a certain noise-buffering capacity (robustness), as soon as the two loops operate on different time scales. Here we explore the properties of the nonlinear system responsible for this behavior. We argue that (a) the noise buffering is not linked to the stochastic nature of the stimulus, but only to the time scale of the stimulus variation compared to the intrinsic time scales of the system, and (b) this buffering of stimulus variations follows from the stabilization of a region of the state space away from the equilibrium branches of the system. Our analysis is based on a slow-fast decomposition of the dynamics. We analyze the strength of this buffering as a function of the time scales involved and the Boolean logic of the coupling between dynamic variables, as well as of the amplitude of the stimulus variations. We underline that such a nonequilibrium regime is universal as soon as the stimulus time scale is smaller than the larger time scale of the system, preventing the prediction of the behavior from the features of the bifurcation diagram or using a linear analysis.

*Keywords*: Feedback loops; incomplete bifurcation; noise buffering; slow-fast decomposition.

## 1. Introduction

### 1.1. *Background*

Motivated by graph theory and nonlinear dynamics, an influential trend of research in systems biology currently attributes properties of biological function to specific regulatory motifs [Brandman & Meyer, 2008; Novak & Tyson, 2008]. Examples include circuits of negative feedback loops [Pigolotti *et al.*, 2007], interlinked feedback loops acting on different time scales [Brandman *et al.*, 2005], regulatory devices capable of adaptation [Ma *et al.*, 2009], the composition of a system out of regulatory units [Milo *et al.*, 2004] and their relation to robustness [Klemm & Bornholdt, 2005; Kaluza *et al.*, 2007; Kaluza & Mikhailov, 2007; Kaluza *et al.*, 2008; Lesne, 2008], and the number of positive and negative feedback loops in regulatory circuits [Kwon & Cho, 2008].

One of the intrinsic challenges such regulatory devices often face is to respond rapidly to some external signal and, at the same time, filter out spurious stimuli and fluctuations arising from the environment.

In the context of gene regulation based on the action of transcription factors, Alon and co-workers [Shen-Orr *et al.*, 2002; Alon, 2007] have argued that feedforward loops, with activation thresholds suitably tuned during biological evolution, can serve as a delay element, where only persistent stimuli lead to an activation of the bottom-level element in the feedforward loop, while spurious, noise-like stimuli get filtered out by the consistency check between the other two elements.

Based on a broad range of examples from cell biology, Brandman and co-workers [Brandman *et al.*, 2005] proposed that a frequent motif in signaling, two interlinked positive feedback loops, which act on different time scales, may serve the dual purpose to unite sensitivity and robustness to noise. They supported their hypothesis by a qualitative analysis of numerical simulations obtained with a minimal model of such interlinked feedback loops (see next section for more details on this model). However, they did not provide an analysis of the underlying dynamical mechanism at work. We here reanalyze the observations from [Brandman *et al.*, 2005] using the general framework of slow-fast decomposition.

Given the dynamics producing a bistable switch, as is typically obtained from a positive feedback loop [Thomas & Kaufman, 2001], we want to understand the influence of the different time scales in the dynamics. The observable we analyze is the system response to a step-wise, oscillatory or noisy stimulus. We conduct an analytical and numerical study to better understand the interplay of the time scales involved.

### 1.2. *Minimal model of interlinked feedback loops*

Figure 1 shows the detailed architecture of the system from [Brandman *et al.*, 2005], including production and degradation terms for the internal species $A$, $B$, and the output $X$. Following [Brandman *et al.*, 2005], the model is organized in such a way that the time scales of degradation of $A$ and $B$ coincide with the parameters $\tau_A$ and $\tau_B$, respectively, and that feedback of the output on both $A$ and $B$ are nonlinear Hill-type functions. In the parameter regime discussed in [Brandman *et al.*, 2005] the system displays bistability as a function of the stimulus strength, serving as bifurcation parameter. A stimulus $S$ acts multiplicatively on the activation terms of the internal species. For our investigation, $S$ serves as a control parameter of the nonlinearity. The stimulus $S$ acts on both $A$ and $B$ and is relayed by their respective dynamics

$$\frac{dX}{dt} = \tau_X^{-1}\left[k_{X,\mathrm{on}}(1-X)\left(\frac{A+B}{2}\right)^{n} - k_{X,\mathrm{off}}X + k_{X,\mathrm{min}}\right] \tag{1}$$

$$\frac{dA}{dt} = \tau_A^{-1}\left[S(1-A)\left(\frac{X^n}{X^n + ec_{50}^n}\right) - A + k_{\mathrm{min}}\right] \tag{2}$$

$$\frac{dB}{dt} = \tau_B^{-1}\left[S(1-B)\left(\frac{X^n}{X^n + ec_{50}^n}\right) - B + k_{\mathrm{min}}\right] \tag{3}$$

with different time scales, e.g. $\tau_B \gg \tau_A$ in the fast–slow case (in any case, when the time scales of $A$ and $B$ are not equal, we choose $B$ to be the slower variable among $A$ and $B$). Note that we have self-inhibitory terms ensuring that all three variables $A$, $B$ and the output $X$ remain bounded.

It should be noted that there are, indeed, four time scales in the system ($\tau_A$ and $\tau_B$, the time scale of the signal, $\tau_S$, and the time scale $\tau_X$ of the evolution of the output variable driven by $A$ and $B$). In [Brandman *et al.*, 2005] the time scale of the output

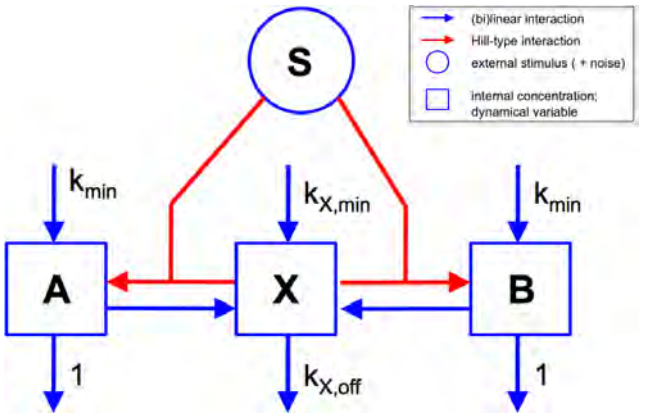


Fig. 1. Schematic representation of the interlinked feedback loop system from [Brandman *et al.*, 2005].

$X$ is implicitly set to $\tau_X = 1$. We shall see below that what matters for the dynamical phenomena mentioned above is $\tau_X \ll \tau_A \leq \tau_B$.

At equilibrium, at fixed $S$, $A(S) = B(S)$, and $X(S)$ is a monotonously increasing function of $A(S) + B(S)$. For suitable values of the parameters, we have three solutions $X^-(S)$, $X^u(S)$ and $X^+(S)$ in some range $S_{\min} < S < S_{\max}$, denoting the lower stable, unstable and upper stable fixed points, respectively. Then necessarily (because at equilibrium, $A$ and $B$ are uniquely determined knowing $S$ and $X$) we also observe three distinct values $A^-(S)$, $A^u(S)$ and $A^+(S)$ (and the same for $B$). The equilibrium curve is thus $S$-shaped in any projection plane and contained in the surface $A = B$. The bifurcation diagram, as well as the nullclines, are the same whatever the values of $\tau_A$, $\tau_B$ and $\tau_X$.

In the following, we plot the theoretical, asymptotic bifurcation diagram, that is the value of the single or two stable fixed points $X^{\pm}(S_0)$ and the unstable fixed point $X^u(S_0)$ as a function of a constant stimulus $S_0$ as a reference, to set the actual simulated trajectories against it. Then we investigate the interplay between the relaxation towards the equilibrium branches of the bifurcation diagrams and the time dependence of the stimulus $S$. Specifically we investigate, how the output is controlled by the three time scales $\tau_X \ll \tau_A \leq \tau_B$ of the system's evolution laws and by the additional time scale $\tau_S$ that comes into play when the stimulus is varying.

Parameter values we are using throughout this paper are (in agreement with [Brandman *et al.*, 2005]): $k_{X,\text{on}} = 2$, $k_{X,\text{off}} = 0.3$, $k_{X,\min} = 0.001$, $k_{\min} = 0.01$, $n = 3$, $ec_{50} = 0.35$, as well as $\tau_A = 2$ for a fast loop and $\tau_B = 125$ for a slow loop. The only difference to the model from [Brandman *et al.*, 2005] is the normalized value of $A + B$ (divided by 2) on the right-hand side of $dX/dt$ so that a single and double loop system would have the same bifurcation diagram. The time scale $\tau_S$ has been taken to be 30 for the stochastic variation (and, for visual clarity, 60 for the deterministic periodic variation discussed below).

Our noise $S(t)$ is a random sequence of steps. The time intervals between steps are drawn from a uniform distribution with an average of 30 and a width of $\pm 10$. The height is drawn from a uniform distribution between 0 and the constant signal strength $S_0$. Apart from wanting to stay as close to the system introduced in [Brandman *et al.*, 2005] on biological grounds, the motivation for the step-like noise on top of the signal is also that it contains only a single dominant time scale.

## 2. Results

### 2.1. *Reproduction of the previous result*

A reproduction of the key finding from [Brandman *et al.*, 2005] is shown in Fig. 2. For three time-scale constellations (first row: slow–slow, that is, $\tau_A = \tau_B = 125 \gg \tau_S$; second row: fast–fast, that is, $\tau_A = \tau_B = 2 \ll \tau_S$; and third row: fast–slow or dual, that is, $\tau_A = 2 \ll \tau_S \ll \tau_B = 125$) the time course (left-hand side) of the output $X$ under the effect of the noisy stimulus and the trajectory in the bifurcation plot (right-hand side) is given. Note that noise is not white noise but a random alternation of positive and negative steps with finite characteristic amplitude $\eta$ (bounded variance) and an average duration $\tau_S$.

By construction, the slow–slow system (top row) fails to respond rapidly enough to the onset of the stimulus and almost fully buffers fluctuations. When both feedback loops are fast, as given in the second row of Fig. 2, the system frequently falls back into the previous fixed point (the one for $S = 0$) under the action of the stimulus noise, following its variation.

The dual case (third row in Fig. 2) is substantially less affected by the noise and, at the same time, is capable of responding to the onset of the stimulus almost as rapidly as the fast–fast system. This is the key feature described in [Brandman *et al.*, 2005]. One question we are addressing here about the mechanism behind the robust functioning of this regulatory device is, how the attribution

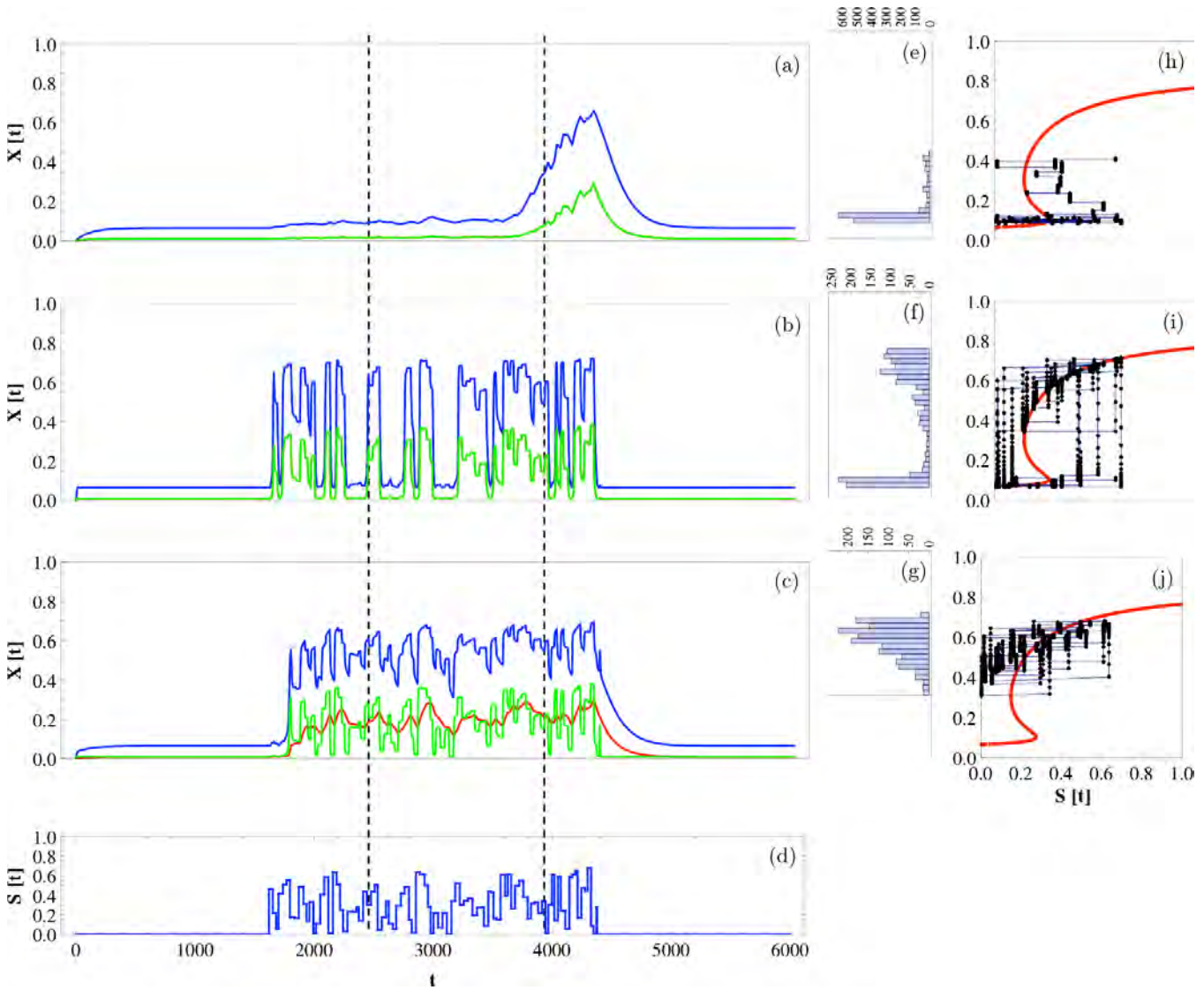


Fig. 2. Reproduction of the simulation results from [Brandman *et al.*, 2005] for the slow–slow case [(a), (e) and (h)] fast–fast case [(b), (f) and (i)], and the dual slow–fast case [(c), (g) and (j)]. The noisy stimulus is presented in (d). The time-course evolution of the output quantity $X$ (designated with blue), along with the quantities $A$ and $B$ (designated with green and red respectively (Note: for the slow–slow and the fast–fast cases those two quantities coincide)) is shown in panels (a), (b) and (c). Panels (e), (f) and (g) give a histogram of values of the output $X$ for a time window from $t = 2500$ to $t = 4000$. These histograms give an indication of the dwelling times of the system at the different output values $X$. In panels (h), (i) and (j), the trajectory of the output $X$ under the effect of the noisy stimulus can be seen in the bifurcation plot for each example (superimposed to the bifurcation diagram shown in red). Dashed lines: window from which the trajectories in (h), (i) and (j) have been taken.

of the two time scales (fast = onset, slow = noise response) is achieved.

Plotting the probability distribution function $P(A, B, X)$ (or its marginal distributions, e.g. $P(X)$, which is approximated by the histograms in Fig. 2) visually captures the evidence of the change in the phase space exploration when the slowest characteristic scale of the evolution, $\tau_B$, increases far beyond the characteristic time $\tau_S$ of the stimulus (middle column frames e, f, g in Fig. 2). What deserves the name of stochastic potential is minus the logarithm of this distribution function [Lemarchand *et al.*, 1988], and it has no direct relation to Kramers rate theory, contrary to what is misleadingly presented in [Zhang *et al.*, 2007]. This representation of the trajectories underline nonequilibrium effects that stabilize other regions than equilibrium branches. This stabilization might give dominant weight to the corresponding regions.

The trajectories in the bifurcation plane essentially characterize the noise buffering observed in [Brandman *et al.*, 2005] as an incomplete relaxation towards the fixed points. This is particularly strong for the lower fixed point. It should be noted that incomplete relaxation is a universal phenomenon, which is, however, frequently ignored. The level of the relaxation is then perceived as the noise buffering capacity of the system. The concept of incomplete relaxation will be explained in more detail in the next section.

### 2.2. *Slow–fast decomposition*

We explore the quantitative properties of the incomplete relaxation and the buffering capacity by means of a slow–fast decomposition.

Slow–fast decomposition refers to a decomposition of $(X, A, B, S)$ into $(y, Z)$ where $y$ is fast and $Z$ slow, i.e. $y$ relaxes fast to a steady state $y^*(Z)$. It amounts to the determination of a so-called slow manifold $\mathcal{W}$, defined by the equation $y = y^*(Z)$, i.e. formed by the points $[y^*(Z), Z]$. Then the dynamics can be reduced to the slow dynamics on the manifold, i.e. the slow evolution of $Z(t)$, to which the evolution of the fast variable(s) $y$ is enslaved. There are possibly more than two levels, namely several nested slower and slower manifolds (the slowest has the smallest dimension and is embedded in other ones).

The vision of a one-dimensional slow manifold parameterized by $S$ (i.e. $Z = S$), and fast variables $y = (A, B, X)$ yields the $S$-shaped bifurcation diagram. Taking this as a reference picture provides valid insights into the dynamics of the system only if $\tau_S$ is far larger than all the time scales of the dynamics, which correspond here to the fast–fast case. In other situations, as soon as $\tau_S \ll \tau_B$, the slow manifold is different and cannot be reached by a nonequilibrium perturbation analysis of the bifurcation diagram nor any linear stability analysis.

Here a central feature is rather the value $\tau_X \ll (\tau_A, \tau_B)$, from which follows that at fixed stimulus $S$, the output $X$ is enslaved to the evolution of the reacting species $A$ and $B$. As soon as[1] $\tau_X \ll \tau_A \leq \tau_B$, the quasi-stationary approximation for $X$ (whatever the stimulus is) yields an enslaving of $X$ to the combination $A + B$, namely

$$X = \phi(A + B) \quad \text{with}$$
$$\phi(z) = \frac{k_{X,\min} + k_{X,\text{on}}\left(\frac{z}{2}\right)}{k_{X,\text{eff}} + k_{X,\text{on}}\left(\frac{z}{2}\right)}. \tag{4}$$

The very first stage of the evolution is a fast convergence of the initial conditions $(A_0, B_0, X_0)$ spread out in a volume to the surface $X = \phi(A + B)$ (slow manifold, see Fig. 4). At fixed $S$, either $\tau_A \sim \tau_B$ and the trajectories will converge on this surface towards the nearest fixed point; or $\tau_A \ll \tau_B$ and the trajectories will first converge to a surface $A = A(B, S)$ enslaved to $B$ at fixed $S$ and embedded in the above-mentioned hyper-surface, Eq. (4), then this surface itself shrinks towards the stable branches of fixed points (parameterized by $S$), as $B$ slowly evolves towards its equilibrium value.

For a varying stimulus, in the dual case $A$ is enslaved to a combination of $S$ and $B$. In the slow–fast or slow–slow cases, the variable $B$ evolves far slower than $S$. It would nevertheless be misleading to consider that $B$ is only sensitive to the time average of $S$ over $\tau_B$: As detailed below for the case of a periodic stimulus, this would ignore the difference between the evolutions of $B$ corresponding to different values of $S$ (due to the fact that in our model the stimulus involved is nonadditive).

### 2.3. *Detailed discussion of time scale regimes and extension to a periodic driver*

It is clear from Fig. 2 that the behavior of the output is determined from the time scale of the stochastic stimulus variation, rather than by the stochasticity itself. In Fig. 3, we therefore substitute the stochastic stimulus by a periodic driver, in order to systematically vary the time scale of the stimulus relative to the time scale present in the ODE system. For clarity, we argue in what follows with a periodic sequence of discrete stimulus jumps between $S = 0$ and $S = S_0 > 0$; our numerical results in Fig. 3 show that the arguments remain valid in the case of a continuous periodic driver.

- *In the fast–fast case* (meaning $\tau_A = \tau_B \ll \tau_S$) $X$, $A$ and $B$ have enough time to experience complete transitions and relax to their equilibrium

[1]The behavior for $\tau_X \geq \tau_B \geq \tau_A$ would be trivial (stabilization to the lower equilbrium point). We are not discussing the case $\tau_A \leq \tau_X \leq \tau_B$.

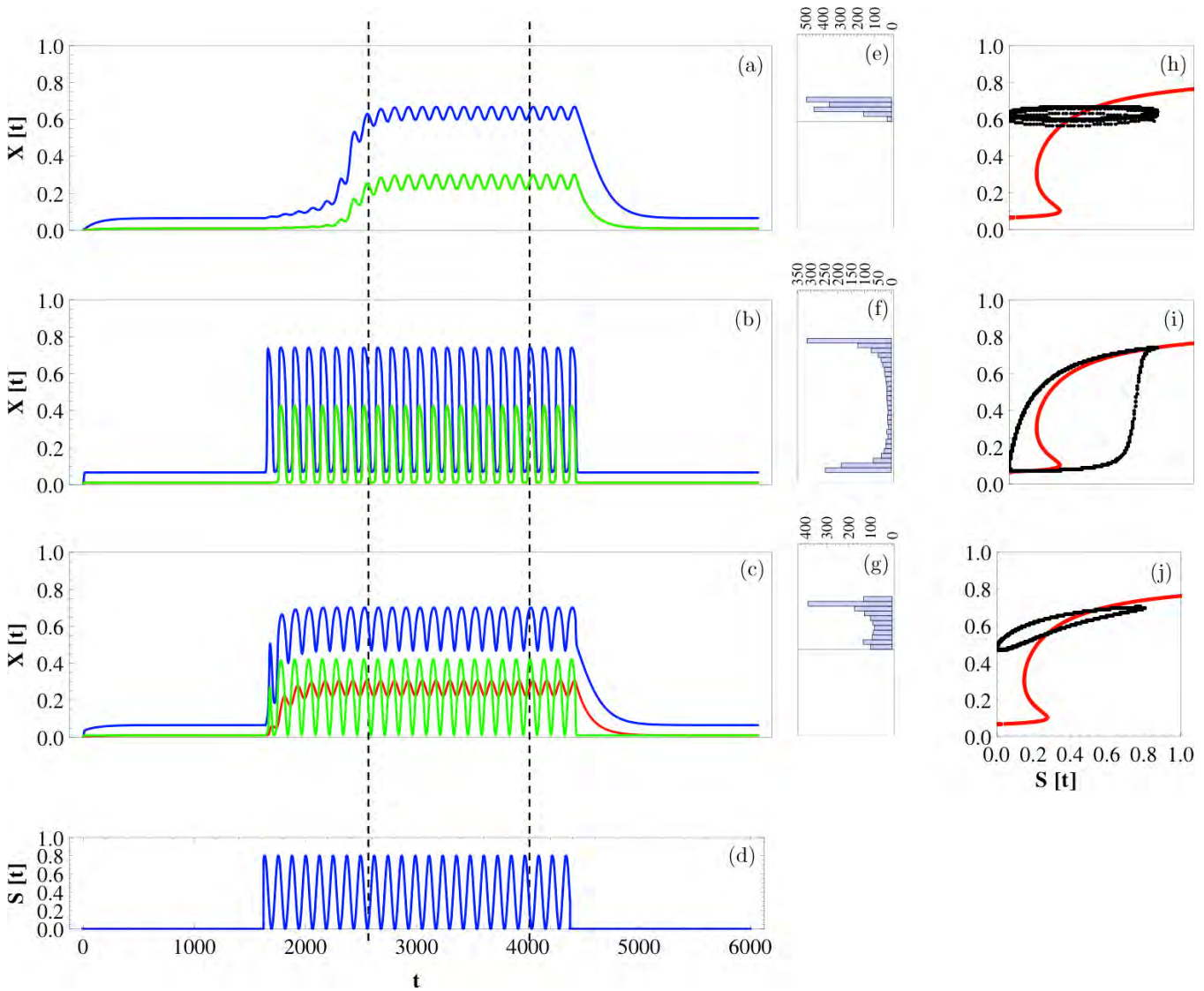


Fig. 3. Same as Fig. 2, but with a periodic deterministic stimulus.

values in between each jump of the stimulus; in particular, they all can be considered as simply enslaved to the stimulus' oscillations.

By contrast, *as soon as* $\tau_S$ *is smaller than* $\tau_B$ *or both,* $\tau_A$ *and* $\tau_B$, the transitions will be incomplete (incomplete bifurcations) and the evolution of the corresponding variables, either $B$ or both $A$ and $B$, will be truncated. $B$ experiences a slow oscillatory drift towards its upper value $B^+(S_0)$, which nevertheless is not reached. The level $B^*$ reached by $B$ in the slow–fast or slow–slow cases corresponds to a perfect balance between the upward and downward steps (see Sec. 2.6 below).

- *In the slow–slow case*, $A$ and $B$ will barely evolve between two jumps of the stimulus. The main point is the asymmetry of the evolution for $S = 0$ and $S = S_0$, the latter being a bit less slower than the former, due to the additional $S_0$-dependent term on the right-hand side of the evolution laws for $A$ and $B$. Hence $A$ and $B$ will evolve a bit more towards their values $A^+(S_0)$ and $B^+(S_0)$ in the phase when $S = S_0$ then they will relax (exponentially fast, with respective characteristic times $\tau_A$ and $\tau_B$) towards their values $A^-(0) = k_{\min}$ and $B^-(0) = k_{\min}$ in the phase when $S = 0$. We henceforth observe for $A$ and $B$ a slow drift towards their values $A^+(S_0)$ and $B^+(S_0)$ (which are not reached) superimposed to oscillations of period $\tau_S$ and small amplitude. In order to distinguish the fixed-point values $A^+(S_0)$ etc. from

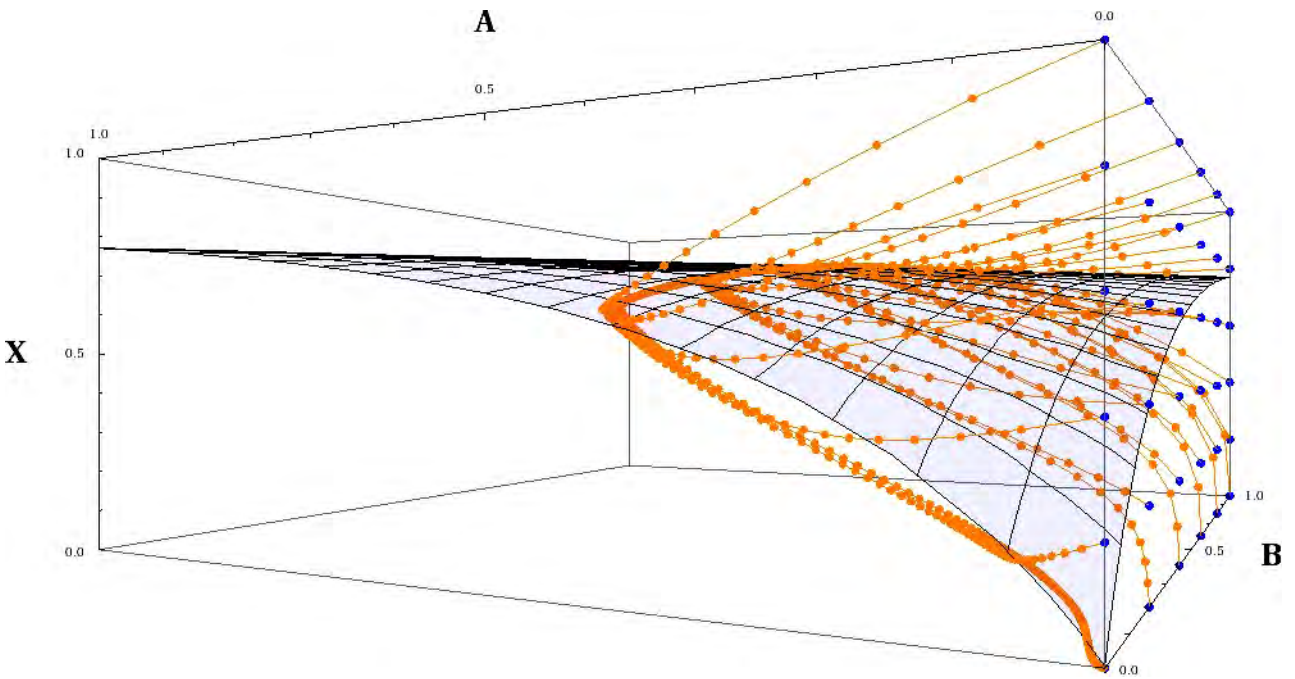


Fig. 4. Relaxation to the slow manifold [obtained from Eq. (4)] of a trajectory in phase space for the dual (slow–fast) system, for a constellation of different initial conditions (shown in blue) spanning the right-hand side of the cube.

the numerical values reached during the oscillatory drift, we denote the latter by $A_{\max}$ (for the upper value of the variation in $A$ observed during the variation of the stimulus) and $A_{\min}$ (for the corresponding lower value). The time average in this regime is denoted by $A^* = (A_{\max} - A_{\min})/2$. Relatedly, $B_{\max}$, $B_{\min}$, and $B^*$ can be defined. The oscillatory drift persists until values $A^*$ and $B^*$, for which steps upwards and downwards equilibrate, are reached. $X$ remains at each moment enslaved to $A + B$.

- *In the slow–fast case*, namely $\tau_X \ll \tau_A \ll \tau_S \ll \tau_B$, one first observes a saw-like transient for $A$, $X$ and above all $B$, the more visible the longer the time scale $\tau_B$. In this transient, steps upwards are larger than the steps downwards. Since $\tau_B \gg \tau_S$, $B$ follows the oscillations with a delay reflected in a phase shift, increasing as $\tau_B$ increases. The same argument as in the slow–slow case remains valid and $B$ will experience a slow drift towards the "balance" value $B^*$ superimposed to oscillations of period $\tau_S$ and small amplitude. Since $\tau_A \ll \tau_S$, $A$ is enslaved to the stimulus and follows almost in phase the oscillation of the stimulus; since $A$ is enslaved not only to $S$ but also to $B$ (via the $X$-dependence of the right-hand side of $dA/dt$), and $B$ experiences delayed and incomplete relaxation, $A$ is not exactly in phase with $S$ and typically does not reach the equilibrium values $A^{\pm}(S)$, but values $A_{\max} < A^+(S)$ and $A_{\min} > A^-(S)$. The output variable $X$ remains enslaved to $A + B$ and accordingly, $X$ exhibits oscillations of period $\tau_S$.

### 2.4. *Asymmetry of the on–off transition*

Due to the details of the system equations (namely the fact that the absolute value of the right-hand side of $dA/dt$ and $dB/dt$ are lower for $S = 0$ than for $S_0$), the incomplete relaxation is more pronounced towards the lower fixed point. From Fig. 3, as well as from its stochastic counterpart, Fig. 2, this asymmetry in the dual system is related to an asymmetry between the transitions towards the upper fixed point and towards the lower fixed point, i.e. an asymmetry between the on-transition and the off-transition.

At $t = 0$, $S$ jumps from $S = 0$ (for $t < 0$) to $S_0 \gg S_{\max}$. The variable $X$ is slaved to $A + B$ and will vary as soon as $A$ or $B$ varies. Plugging in $X = \phi(A+B)$ in the evolution equations for $A$ and $B$ shows that the evolutions of $A$ and $B$ are indirectly coupled as soon as $S > 0$. $X$ will reach its equilibrium value only when $A$ and $B$ have reached their equilbrium values.

When $S$ turns off, $S = 0$, the evolution equations of $A$ and $B$ are

$$\frac{dA}{dt} = \tau_A^{-1}(k_{\min} - A), \quad \frac{dB}{dt} = \tau_B^{-1}(k_{\min} - B).$$

The evolution of $A$ and $B$ are now totally decoupled. The evolution of $X$ is ruled by the slowest of the two variables, here $B$.

This asymmetry contributes to the functional features of the perceived noise buffering.

### 2.5. *Numerical analysis for a system with a multiplicative reaction term*

It is instructive to explore, how the logical coupling between the three dynamical variables, in particular the action of $A$ and $B$ on $X$, affects the buffering capacity. The original system from [Brandman *et al.*, 2005] is based on a logical OR: $\dot{X} = f(A \text{ OR } B)$, suggesting that the on-transition ($S$ switching to a nonzero value $S_0$) is determined by the fast time scale, while the off-transition ($S$ switching to 0) requires both intrinsic variables $A$ and $B$ to go down and therefore is determined by the slow time scale, leading effectively to the incomplete transition towards the lower fixed point and to the observed buffering capacity. In order to investigate, whether this qualitative argument really accounts for the buffering capacity observed here, we exchange the logical OR from the previous model by a logical AND, where $\dot{X} = f(A \text{ AND } B)$. The coupling term in this case is given by $\sqrt{AB}$, instead of $(A+B)/2$. The square-root ensures that the single loop system and the two-loops system have the same bifurcation diagram/equilibrium curve, with moreover $A = B$ at equilibrium. Figure 5 shows the dual system for both logical couplings. It is seen that the buffering capacity is indeed lower for the second model. It is however still clearly visible. Thus, also the model using a logical AND shows an incomplete relaxation towards a lower fixed point.

Assuming $\tau_X \ll \tau_A \leq \tau_B$, we now obtain that $X$ is enslaved to the product of $A$ and $B$, namely $X = \phi(2\sqrt{AB})$. There is also an indirect coupling of the dynamics of reactive species (i.e. of the two loops) due to the common feedback of the enslaved outcome $X = \phi(2\sqrt{AB})$.

### 2.6. *Quantification of noise buffering capacity*

As a first step of quantitatively understanding noise buffering in this system of interlinked feedback loops, we investigate, how well the result of the slow–fast decomposition, Eq. (4) predicts the extreme levels of oscillation of the output $X$ under a periodic driver.

- In the fast–fast case, the minima of $X$ lie at the position $\phi(A^-(0)) = \phi(k_{\min})$, while its maxima lie at the position $\phi(A^+(S_0))$.

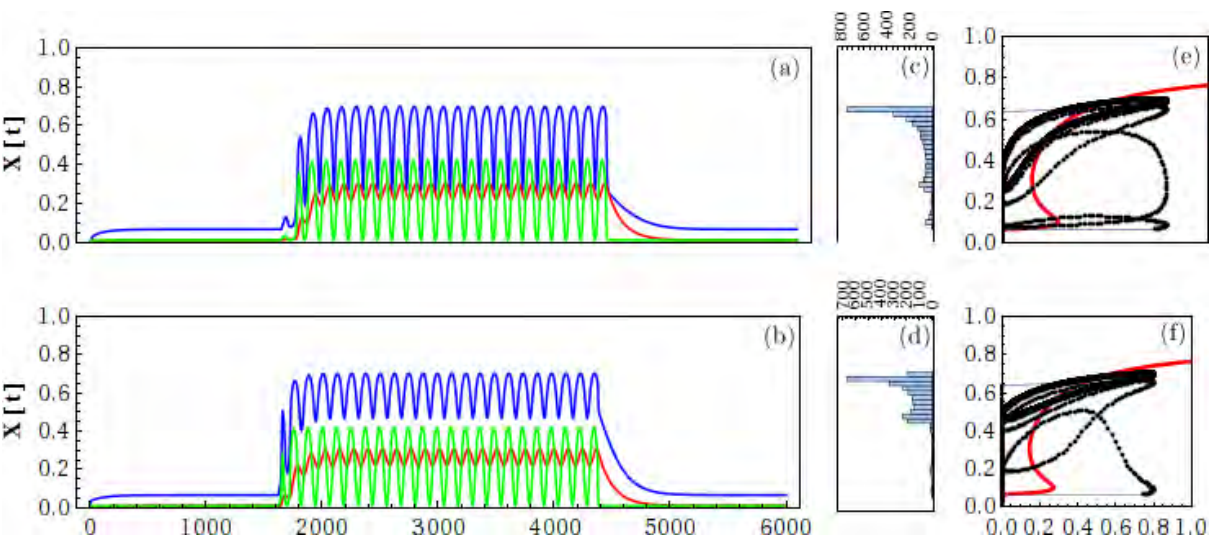


Fig. 5. The response of the feedback loop system with a multiplicative reaction term (logical AND) (upper row) is compared with the case of an additive reaction term (logical OR) (bottom row). Parameter settings are those for the dual (slow–fast) system. For clarity, the time course of the stimulus has been omitted. The bottom row coincides with the corresponding curves from Fig. 3.

- By contrast, in the slow–fast case, the slow variable $B$ does not reach its upper equilibrium value $B^+(S_0)$ nor its lower equilibrium value $B^-(0) = k_{\min}$, but values $B_{\max}(S_0)$ and $B_{\min}(S_0)$ very close to $B^*(S_0)$. Henceforth, neither $A$ nor $X$ will reach their upper and lower equilibrium values, despite the fact that their characteristic times, $\tau_A$ and $\tau_X$, respectively, are small compared to the stimulus period $\tau_S$. The minima of $A$ during oscillations of the stimulus between $S = 0$ and $S = S_0$ can be related to the maxima $A_{\max}(S_0)$ by integrating the evolution law for $A$ when $S = 0$; it yields a minimum value

$$A_{\min}(S_0) = k_{\min} + (A_{\max}(S_0) - k_{\min})e^{-\tau_S/\tau_A},$$

  which is very close to $k_{\min}$ as soon as $\tau_A \ll \tau_S$. Note that we here recover the asymmetry between the on–off and off–on transitions discussed in Sec. 2.4: whereas $A_{\max}$ depends on $S_0$, $A_{\min}$ takes a value in practice independent of $S_0$. As for $X$, it oscillates between the value $\phi(k_{\min} + B^*(S_0))$ and the value $\phi(A_{\max}(S_0) + B^*(S_0))$.
- In the slow–slow case, a similar reasoning as in the dual case, but now for both $A$ and $B$, accounts for oscillations of $A$, $B$ and $X$ having the period $\tau_S$ of the stimulus and weak amplitudes around respectively $A^*(S_0)$, $B^*(S_0) = A^*(S_0)$ and $X^*(S_0) = \phi(A^*(S_0))$, as seen in Fig. 3. The whole discussion remains valid for the AND logical coupling rule, provided we replace $X = \phi(A + B)$ by $X = \phi(2\sqrt{AB})$.

The system is thus stuck at or in between $S_0$-dependent positions. Summarizing, it is thus clearly seen from the numerical simulations that the behavior of the system, and in particular that of the slow–fast case, is not stochastically determined but rather incorporated in the system's architecture.

Figure 6 shows this prediction of the noise buffering capacity (given by the amplitude

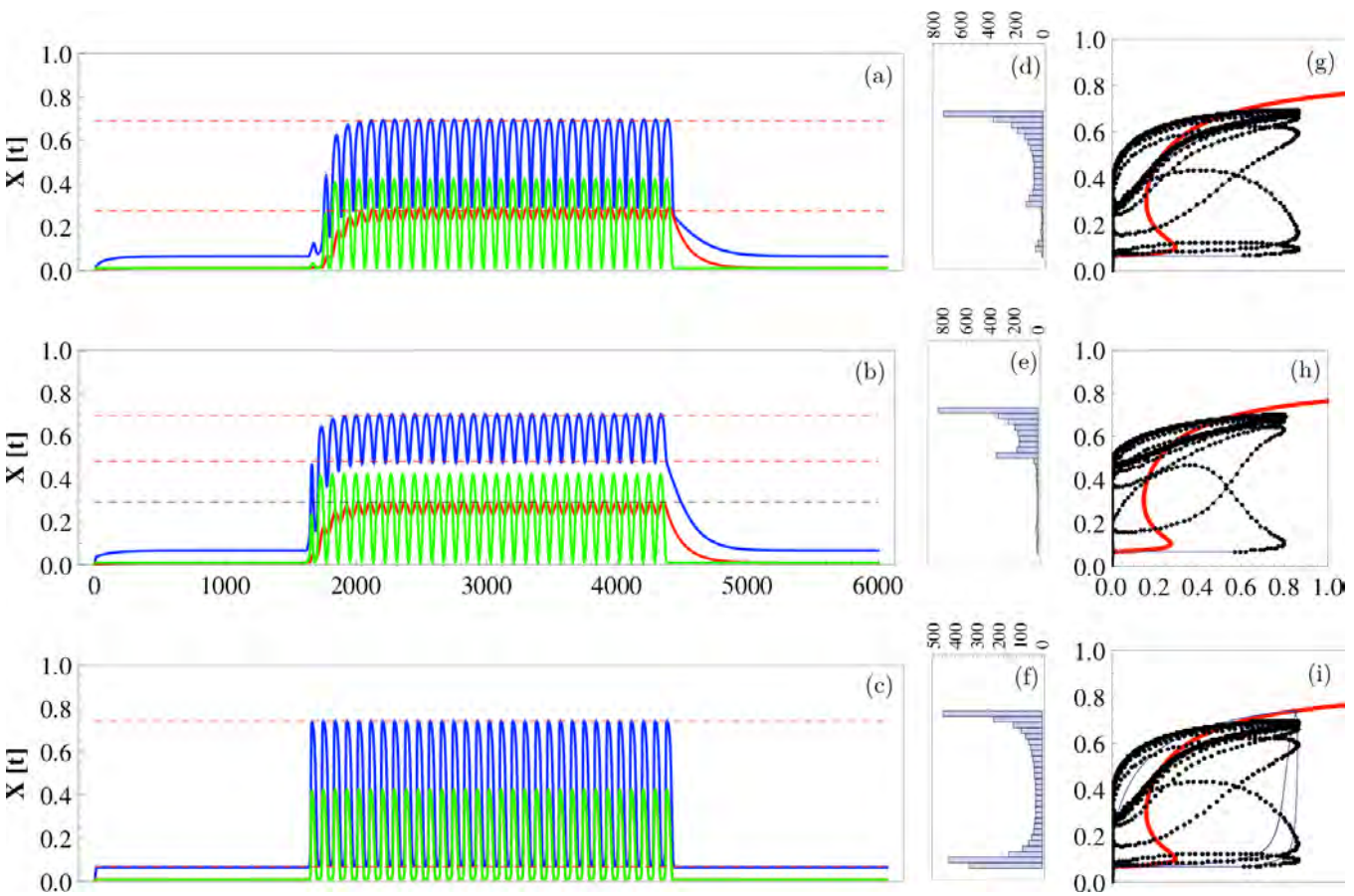


Fig. 6. For several of the previous response patterns, the prediction (dashed red line) from Eq. (4) (or its corresponding version $X = \phi(2\sqrt{AB})$ for a multiplicative reaction term) has been inserted. Row 1: multiplicative reaction term for the slow–fast system (same as Fig. 5, top row); row 2: additive reaction term for the slow–fast system (same as Fig. 5, bottom row); row 3: multiplicative reaction term for the fast–fast system. Again, for clarity, the time course of the stimulus has been omitted.

reduction of the output variable) inserted in some of the previous response patterns.

We can go one step further in the prediction of the noise buffering by looking at the value of $B^*$ reached by $B$ in the slow–fast or slow–slow cases, when the oscillatory upwards drift has stabilized. Explicitly, it is obtained by writing that the steps upward and downward made at each half-period of the stimulus equilibrate. The Hill function $h(x) = x^n/(x^n + ec_{50}^n)$ with $n = 3$ is a steep sigmoidal with an inflexion point at $X_0 = ec_{50}$. Accordingly, we shall approximate $h(x) \approx 0$ if $x < ec_{50}$ and $h(x) \approx 1$ if $x > ec_{50}$. We shall assume that the output oscillates between sufficiently large values to replace $h(X)$ by 1. Also, we shall use a linear approximation of the dynamics around the searched value $B^*$, namely consider that the step upwards (for the variable $B$) has roughly an amplitude of $(\tau_S/2\tau_B)[dB/dt(S_0)]$ and that the step downwards has roughly an amplitude of $(\tau_S/2\tau_B)[dB/dt(S = 0)]$. It thus becomes $S_0(1 - B^*) \approx 2[B^* - k_{\min}]$, yielding

$$B^* \approx \frac{S_0 + k_{\min}}{S_0 + 2}. \tag{5}$$

It is easy to check that $B^* < B^+(S_0)$ (note that $B^*$ also depends on $S_0$ and should be denoted $B^*(S_0)$). Rigorously, around $B^*(S_0)$, we should have $\int_0^{\tau_S/2} dB/dt(S_0)\,dt = -\int_0^{\tau_S/2} dB/\mathrm{dt}(0)\,dt$. Note that Eq. (5) is valid whether we consider OR and AND logical rules for describing the influence of $A$ and $B$ on $X$. This balance value, at least its approximate value does not depend on the time scale $\tau_B$ provided $\tau_B \gg \tau_S$.

## 3. Discussion

The dominant functional feature of this regulatory device, namely the combination of a rapid response to the onset of the stimulus and a buffering of noise, is not a consequence of the stochasticity of the external stimulus. It is rather linked to the time scale separation among the dynamical variables and with respect to the stimulus variation (independently of whether this variation is stochastic or periodic).

Time scales here really determine the functional features of the system. In particular, the "equilibrium view" associated with the bifurcation diagram is misleading, as soon as the stimulus time scale is smaller than the larger time scale of the system. Whether the varying stimulus is deterministic or stochastic does not matter for these features. This, moreover, endows the system with out-of-equilibrium features, since it might now spend noticeable time in the neighborhood, e.g. of the metastable branch, whereas it would never visit the upper and the lower fixed points (equilibria).

A similar behavior like in the dual system discussed here is also observed in a coherent feedforward loop. The coherent feedforward loop is a frequent network motif of, e.g. gene regulatory networks, where a general transcription factor $X$ regulates an effector operon $Z$ directly and via a specific transcription factor $Y$ [Alon, 2007; Milo *et al.*, 2004; Shen-Orr *et al.*, 2002]. The two signals are, e.g. combined with a logical AND to yield the output state of $Z$. Coherence here means that both routes from $X$ to $Z$ have the same sign (either activating or inhibitory). For a suitable choice of activation thresholds, this device is capable of filtering out transient activation signals and responding only to persistent signals, while ensuring a rapid system shutdown when the input stimulus stops [Alon, 2007]. This asymmetry is opposite to the one we observe in our case: The off–on transition is rapid whereas the on–off transition is slow.

In fact, the feedforward loop can be viewed as a stylized representation of such time scale separations. The threshold for $Y$ with respect to $X$ induces a time window for the blocking of the external signal. Fluctuations on a smaller time scale are buffered by the system.

Lastly, it should be noted that it can be very interesting to explore this device also under the influence of a real stochastic driver, using the whole toolbox of stochastic processes. In particular, when the noise is tuned to induce jumps across the unstable branch, one could in principle observe the exact opposite effect for the dual system: an amplification of the noise in the system output via on–off intermittency [Aumaître *et al.*, 2005].

## Acknowledgments

M. Hütt acknowledges the stimulating discussions on interlinked feedback loops with Ala Trusina (Copenhagen/Denmark), while he was visiting the Center for Models of Life at Niels Bohr Institute. He also acknowledges the generous support from the IHÉS guest program for the purpose of this work; A. Lesne has been a visitor of the ICTS program at Jacobs University during the initial phase of this work.

## References


Alon, U. [2007] "Network motifs: Theory and experimental approaches," *Nat. Rev. Genet.* **8**, 450–461.

Aumaître, A., Pétrélis, F. & Mallick, K. [2005] "Low-frequency noise controls on–off intermittency of bifurcating systems," *Phys. Rev. Lett.* **95**, 064101.

Brandman, O., Ferrell, J. E., Li, R. & Meyer, T. [2005] "Interlinked fast and slow positive feedback loops drive reliable cell decisions," *Science* **310**, 496–498.

Brandman, O. & Meyer, T. [2008] "Feedback loops shape cellular signals in space and time," *Science* **322**, 390–395.

Kaluza, P., Ipsen, M., Vingron, M. & Mikhailov, A. S. [2007] "Design and statistical properties of robust functional networks: A model study of biological signal transduction," *Phys. Rev. E* **75**, 015101.

Kaluza, P. & Mikhailov, A. S. [2007] "Evolutionary design of functional networks robust against noise," *Europhys. Lett.* **79**, 48001.

Kaluza, P., Vingron, M. & Mikhailov, A. S. [2008] "Self-correcting networks: Function, robustness, and motif distributions in biological signal processing," *Chaos* **18**, 026113.

Klemm, K. & Bornholdt, S. [2005] "Topology of biological networks and information processing," *PNAS* **102**, 18414–18419.

Kwon, Y.-K. & Cho, K.-H. [2008] "Quantitative analysis of robustness and fragility in biological networks based on feedback dynamics," *Bioinformatics* **24**, 987–994.

Lemarchand, A., Lemarchand, H. & Sulpice, E. [1988] "Interaction of a Hopf bifurcation and a symmetry-breaking bifurcation: Stochastic potential and spatial correlations," *J. Stat. Phys.* **53**, 613–654.

Lesne, A. [2008] "Robustness: Confronting lessons from physics and biology," *Biol. Rev.* **83**, 509–532.

Milo, R., Itzkovitz, S., Kashtan, N., Levitt, R., Shen-Orr, S., Ayzenshtat, I., Sheffer, M. & Alon, U. [2004] "Super-families of evolved and designed networks," *Science* **303**, 1538–1542.

Novak, B. & Tyson, J. J. [2008] "Design principles of biochemical oscillators," *Nat. Rev. Mol. Cell Biol.* **9**, 981–991.

Pigolotti, S., Krishna, S. & Jensen, M. H. [2007] "Oscillations in negative feedback loops," *PNAS* **104**, 6533–6537.

Shen-Orr, S., Milo, R., Mangan, S. & Alon, U. [2002] "Network motifs in the transcriptional regulation network of *Escherichia coli*," *Nat. Genet.* **31**, 64–68.

Thomas, R. & Kaufman, M. [2001] "Multistationarity, the basis of cell differentiation and memory. I. Structural conditions of multistationarity and other nontrivial behavior," *Chaos* **11**, 170–179.

Wenzhe Ma, W., Trusina, A., El-Samad, H., Lim, W. A. & Tang, C. [2009] "Defining network topologies that can achieve biochemical adaptation," *Cell* **138**, 760–773.

Zhang, X. P., Cheng, Z., Liu, F. & Wang, W. [2007] "Linking fast and slow positive feedback loops creates and optimal bistable swtich in cell signaling," *Phys. Rev. E* **76**, 031924.